Antitumor activity of a pyrrole-imidazole polyamide

Fei Yang[a], Nicholas G. Nickols[a,b], Benjamin C. Li[a], Georgi K. Marinov[c], Jonathan W. Said[d], and Peter B. Dervan[a,1]

[a]Division of Chemistry and Chemical Engineering, and [c]Division of Biology, California Institute of Technology, Pasadena, CA 91125; and [b]Department of Radiation Oncology and [d]Department of Pathology and Laboratory Medicine, David Geffen School of Medicine of the University of California, Los Angeles, CA 90095

Contributed by Peter B. Dervan, December 17, 2012 (sent for review October 19, 2012)

Many cancer therapeutics target DNA and exert cytotoxicity through the induction of DNA damage and inhibition of transcription. We report that a DNA minor groove binding hairpin pyrrole-imidazole (Py-Im) polyamide interferes with RNA polymerase II (RNAP2) activity in cell culture. Polyamide treatment activates p53 signaling in LNCaP prostate cancer cells without detectable DNA damage. Genome-wide mapping of RNAP2 binding shows reduction of occupancy, preferentially at transcription start sites, but occupancy at enhancer sites is unchanged. Polyamide treatment results in a time- and dose-dependent depletion of the RNAP2 large subunit RPB1 that is preventable with proteasome inhibition. This polyamide demonstrates antitumor activity in a prostate tumor xenograft model with limited host toxicity.

minor groove binder | small molecule transcription inhibitor | ChIP-Seq

Several chemotherapeutics, including the anthracyclines and cisplatin, exert part of their cytotoxicity through the inhibition of transcription (1). Transformed cells often require constant expression of antiapoptotic genes for survival, making transcription inhibition a relevant therapeutic strategy in oncology (1, 2). Many radio- and chemotherapy treatments that target DNA, including UV irradiation, cisplatin, and the topoisomerase inhibitors, introduce obstacles to RNA polymerase II (RNAP2) elongation by generating bulky or helix-distorting lesions (3–5). In cell culture experiments, transcription blockade has been shown to induce degradation of the RNAP2 large subunit (RPB1), and function as a signal for p53-mediated apoptosis (6, 7). Although many DNA-targeted therapeutics effectively inhibit transcription and induce apoptosis, clinical treatment with genotoxic agents can also damage DNA in normal cells, increasing symptomatic toxicity and potentially leading to secondary cancers (8). The question arises whether high-affinity, noncovalent DNA-binding ligands offer an approach to transcription inhibition without DNA damage.

Hairpin pyrrole-imidazole (Py-Im) polyamides are synthetic oligomers with programmable sequence recognition that bind the minor groove of DNA with high affinity (9). Py-Im polyamide-DNA binding induces allosteric changes in the DNA helix that can interfere with protein–DNA interactions (10, 11). Py-Im polyamides have been used as molecular probes in cell culture to modulate inducible gene-expression pathways (12–15). In rodents, eight-ring hairpin Py-Im polyamides circulate in blood for several hours after administration and affect changes in gene expression in tissues (16–18).

We have previously reported that polyamide **1** (Fig. 1), which targets the sequence 5′-WGWWCW-3′ found in the androgen response element, inhibited a subset of dihydrotestosterone (DHT)-induced genes in LNCaP cells (12). In this article we explore the effects of this polyamide on the RNAP2 transcription machinery. We find that RNAP2 is preferentially reduced from transcription start sites genome-wide without significant perturbation at enhancer loci. This reduction is accompanied by proteasome-dependent degradation of RPB1. Polyamide treatment induces p53 accumulation that is consistent with what is observed for other transcription inhibitors that interact with DNA (4, 5), but without evidence of DNA damage. This polyamide demonstrates efficacy in vivo against prostate cancer xenografts in mice with limited host toxicity.

Results

Effects of Polyamide 1 on Global Occupancy of RNAP2. Polyamide **1** was previously shown to inhibit the induction of a subset of DHT-driven genes in LNCaP cell culture (12). We interrogated the effects of **1** on the RNAP2 transcription machinery by mapping the global occupancy of RNAP2 using ChIP-seq. Under DHT induction, select androgen receptor (AR)-driven genes, such as *KLK3*, showed increased RNAP2 occupancy over genic regions, but this was decreased in the presence of **1** (Fig. 2*A*). Although RNAP2 occupancy across constitutively expressed genes, such as *GAPDH*, did not change with DHT induction, cotreatment with **1** reduced RNAP2 occupancy across these genes (Fig. 2*B*). This reduction in RNAP2 occupancy by **1** was in the context of a global decrease of RNAP2 occupancy across genic regions (Fig. S1), particularly at transcription start sites (Fig. 2*C*). However, **1** did not significantly change RNAP2 occupancy at enhancer loci (Fig. 2*D*), suggesting **1** may affect the active elongation of RNAP2 without disturbing the transcription apparatus anchored at enhancers, and that the observed differences in RNAP2 occupancy are not a result of technical variation in ChIP success between experiments. Reduction in DNA occupancy of RNAP2 has also been reported in cells treated with α-amanitin, a cyclic octapeptide inhibitor of RPB1 (19).

Inhibition of RNAP2 elongation can be caused by a multitude of genotoxic agents and often results in the degradation of the RPB1 subunit (3, 20, 21). Indeed, in addition to reduced RNAP2 DNA occupancy, immunoblot analysis of LNCaP cells treated with **1** shows depletion of RPB1 in a time- and concentration-dependent manner (Fig. 2*E*). To examine if the effect on RPB1 protein were a result of decreased transcription of this gene, we measured levels of RPB1 mRNA (Fig. 2*F*). The expression of RPB1 modestly increased with polyamide treatment, suggesting this depletion is posttranscriptional.

Polyamide Cytotoxicity Is Reduced by Proteasomal Inhibition and Serum Starvation. Inhibition of RNAP2 has been reported to induce apoptosis (4, 6, 22), and may contribute to polyamide cytotoxicity observed in LNCaP cells cultured with **1** (Fig. 3*A*). A previous study with trabectidin, a DNA minor groove alkylator that causes RPB1 degradation, showed the toxicity induced by the molecule can be reduced by cotreatment with the proteasome inhibitor MG132 (22). To evaluate if polyamide-induced toxicity was also reducible by proteasomal inhibition we treated

Author contributions: F.Y., N.G.N., G.K.M., and P.B.D. designed research; F.Y., N.G.N., B.C.L., and J.W.S. performed research; F.Y., N.G.N., and B.C.L. contributed new reagents/analytic tools; F.Y., N.G.N., B.C.L., G.K.M., and P.B.D. analyzed data; and F.Y., N.G.N., and P.B.D. wrote the paper.

The authors declare no conflict of interest.

Freely available online through the PNAS open access option.

Data deposition: The data reported in this paper have been deposited in the Gene Expression Omnibus (GEO) database, www.ncbi.nlm.nih.gov/geo (accession no. GSE43253).

[1]To whom correspondence should be addressed. E-mail: dervan@caltech.edu.

This article contains supporting information online at www.pnas.org/lookup/suppl/doi:10.1073/pnas.1222035110/-/DCSupplemental.

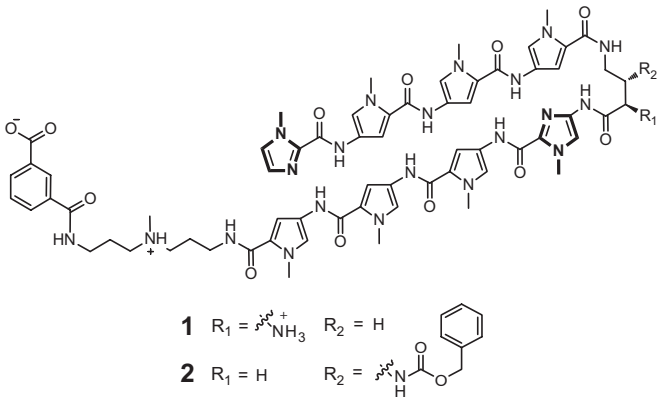

Fig. 1. Structure of polyamides **1** and **2**.

LNCaP cells with **2** in the presence and absence of MG132. We developed analog **2** specifically for this application because prolonged incubation with MG132 alone is cytotoxic, and conjugation of an aryl group to the γ-aminobutyric acid turn have been shown to improve cellular uptake and cytotoxicity of polyamides. Cell-viability experiments showed that **2** induced cell death more rapidly than **1** without significant change to DNA binding (Fig. S2 *A* and *B*). Cell culture experiments revealed coincubation with MG132 reduced cytotoxicity induced by **2** (Fig. 3*B*) and prevented degradation of RPB1 (Fig. 3*C*). Polyamide nuclear uptake was not affected by MG132 (Fig. S2 *C* and *D*). In addition, cytotoxicity studies of cells treated with UV radiation and α-amanitin have shown increased cellular sensitivity to transcription inhibition upon S-phase entry (6, 23). Similarly, **2** was less toxic to LNCaP cells arrested in G_1/G_0 by serum starvation compared with cells grown in normal media (Fig. 3*D* and Fig. S2*E*).

Accumulation of p53 and Expression of p53 Targets in the Absence of DNA Damage. Previously published microarray data of LNCaP cells cotreated with DHT and **1** revealed the induction of several p53 target genes (12). Despite depletion of RPB1, treatment of LNCaP cells with **1** alone induced expression of p53 genes that are characteristic of genotoxic stress (Fig. 4*A*) (24). Many of these genes were previously observed to be induced in A549 cells treated with polyamide as well as polyamide-alkylator conjugates (14, 25). To examine if direct DNA damage was contributing to p53 activity, we looked for evidence of DNA damage in LNCaP cells after extended treatment with **1**. Alkaline comet assay showed no evidence of DNA fragmentation (Fig. 4*B*). Additionally, treatment with **1** did not induce cellular markers of DNA damage, including phosphorylation of γH2A.X, ATM, DNA-PKcs, p53, or Chk2 (Fig. 4*C*). However, modest accumulation of p53 and poly(ADP-ribose) polymerase (PARP) cleavage were observed. These data suggest that **1** activates p53 through transcriptional inhibition without DNA damage, a mechanism that has been observed for non-DNA targeting agents that exert transcriptional stress such as the protein kinase inhibitor 5,6-dichlorobenzimidazole (DRB) and α-amanitin (5, 6, 26).

Effects of Polyamide Treatment on Prostate Cancer Xenografts. We recently reported the toxicity and pharmacokinetic (PK) profile of **1** in mice (17). Subcutaneous injection of **1** also results in detectable circulation (Fig. S3). We thus selected this molecule for further testing against xenografts in vivo. Male NOD scid-γ (NSG) mice bearing LNCaP xenografts were treated with either vehicle or 20 nmol (~1 mg/kg) **1** by subcutaneous injection once every 3 d for a cycle of three injections. At the experimental end point, mice treated with **1** had smaller tumors and lower serum

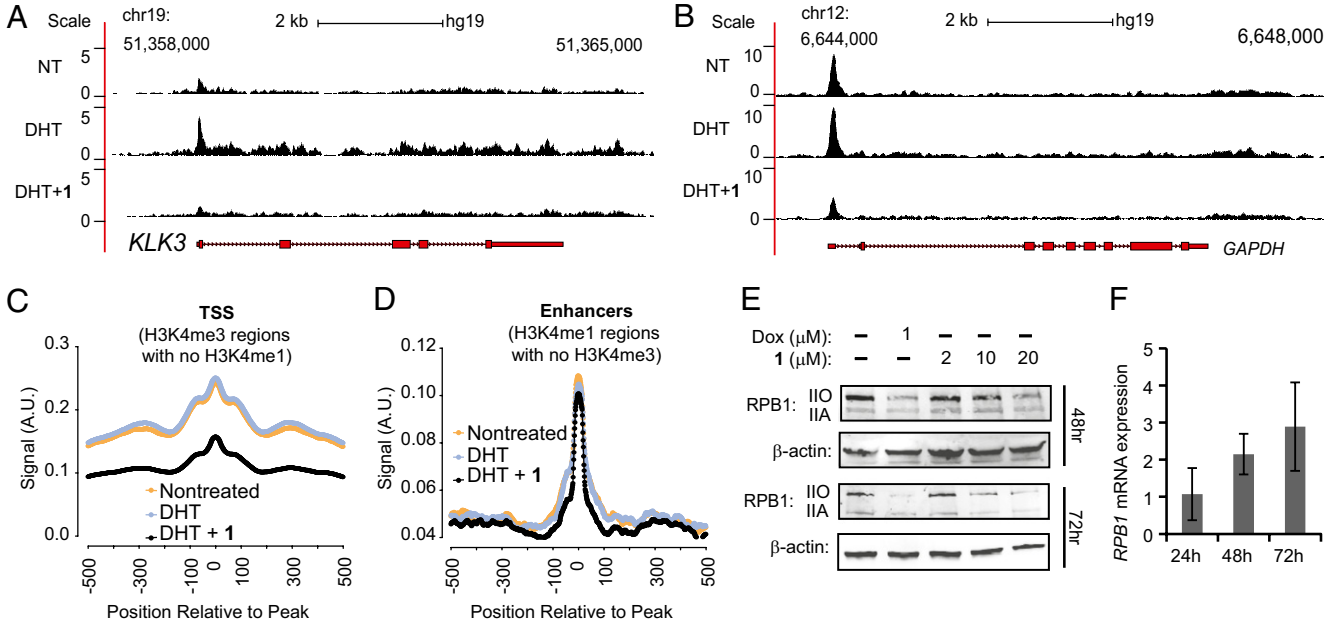

Fig. 2. Global effects of **1** on RNAP2. Genome browser tracks of RPB1 occupancy from untreated, DHT-treated, and DHT + **1**-treated samples over (*A*) an AR-driven gene, *KLK3* (PSA), and (*B*) a housekeeping gene, *GAPDH*. RNAP2 occupancy is mapped as reads per million. (*C*) Genomic RNAP2 occupancy at transcription start sites show comparable levels of enrichment for nontreated and DHT treated samples. Samples treated with DHT + **1** exhibited much lower occupancy. (*D*) Genomic RNAP2 occupancy at enhancer regions is largely unchanged between the three treatment conditions. (*E*) Immunoblot of RPB1 protein in LNCaP cells treated with 1 μM doxorubicin (dox) for 16 h, or **1** at 2 μM, 10 μM, and 20 μM for 48 and 72 h. (*F*) Quantitative RT-PCR measurement of RPB1 transcript levels after LNCaP cells are treated with 10 μM **1** for the indicated times. Relative expression is normalized against nontreated cells. Data represent mean ± SD of biological quadruplicates.

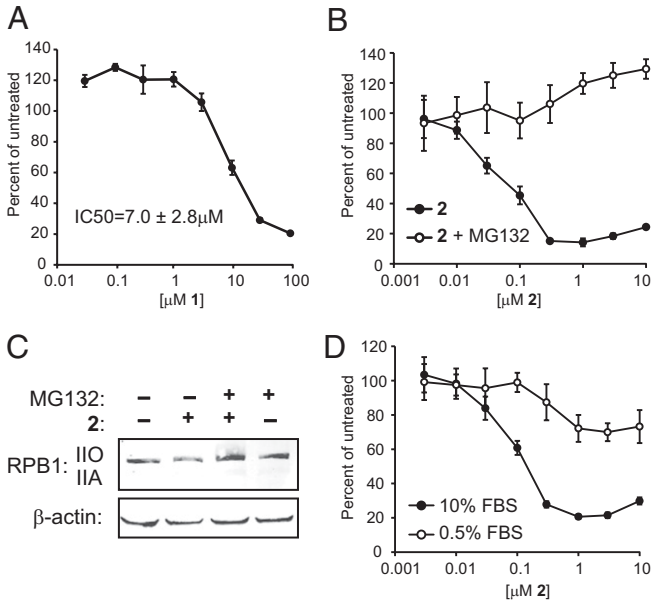

Fig. 3. Cytotoxicity of **1** and **2** and effects on RPB1. (*A*) Cytotoxicity of **1** in LNCaP cells after incubation with **1** for 72 h. Data represent mean ± SD. IC_{50} is calculated from three independent experiments and the error is a 95% confidence intervals. (*B*) Cell viability at 24 h of LNCaP cells treated with varying concentrations **2** with and without proteasome inhibitor MG132 (3 μM, 24 h); proteasome inhibition reduces cytotoxicity of **2**. (*C*) Immunoblot of RPB1 protein in LNCaP cells treated with 10 μM **2** for 12 h followed by 10 μM MG132 for 4 h. (*D*) Cytotoxicity of **2** in LNCaP cells incubated with 10% FBS or with 0.5% FBS for 24 h. Serum starvation decreases percent of cells in the S phase from 8.5% to 4.4% (Fig. S2). Data represent mean ± SD.

prostate-specific antigen (PSA) compared with vehicle controls (Fig. 5 *A* and *B*). Immunohistological analysis of selected tumors showed evidence of cell death by TUNEL stain (Fig. 5*C*). Although tumor-free NSG mice treated with **1** under this regimen showed no signs of distress or weight loss, LNCaP tumor-bearing NSG mice exhibited weight loss by the experimental end point (Fig. S4). This weight loss was accompanied by an elevation in serum uric acid that was not observed in either control group (Fig. 5*D*).

Discussion

DNA targeting agents, including cisplatin, the anthracyclines, minor groove binders, and UV radiation have been demonstrated to affect a multitude of DNA-dependent enzymes, such as the RNA polymerases, DNA polymerase, topoisomerases, and helicases (21, 27). Our research group and others have used polyamides as molecular tools to modulate gene-expression programs (12–15). The programmable sequence specificity of Py-Im polyamides offers a unique mechanism to target specific transcription factor–DNA interfaces and thereby modulate particular gene-expression pathways. In previous studies we have focused our analysis on specific changes to inducible pathways of gene expression. For example, we have shown polyamide **1** affects ~30% of the DHT-induced transcripts in LNCaP cells, which may result from inhibition of the transcription factor AR-DNA interface (12). However, the cellular cytotoxicity of this polyamide may not only be a result of inhibition of DHT-induced gene expression because analogs of **1** exhibit toxicity in a variety of cancer cells (28). It is more likely that polyamides perturb multiple DNA-dependent cellular processes (transcription, replication) that contribute to cytotoxicity. In this study we show that **1** interferes with RNAP2 elongation resulting in the degradation of RPB1, activation of p53, and triggering of apoptosis, without detectable genomic damage.

Our previous study has shown polyamide **1** decreased the expression of a large number of genes in LNCaP cells (12). To examine the effect of **1** on the transcription machinery, we performed genome-wide mapping of RNAP2 occupancy by ChIP-seq. We found that although DHT induction increased RNAP2 occupancy at select AR-driven genes, cotreatment with **1** caused a genome-wide decrease of RNAP2 occupancy across genic regions. The effect was most pronounced at transcription start sites. Interestingly, RNAP2 occupancy at enhancer loci, where the transcription assemblies may be attached via contacts through other proteins, was not significantly affected by polyamide treatment. This finding suggests polyamide **1** may preferentially affect RNAP2 loading at regions where RNAP2 is actively engaged, a mechanism that has been previously proposed for the gene regulatory activity of polyamides (29).

The displacement of RNAP2 from DNA is caused by many DNA damaging agents that pose an impediment to RNAP2 elongation. This effect is normally coupled with the degradation of the large RNAP2 subunit RPB1. Indeed, the cellular level of

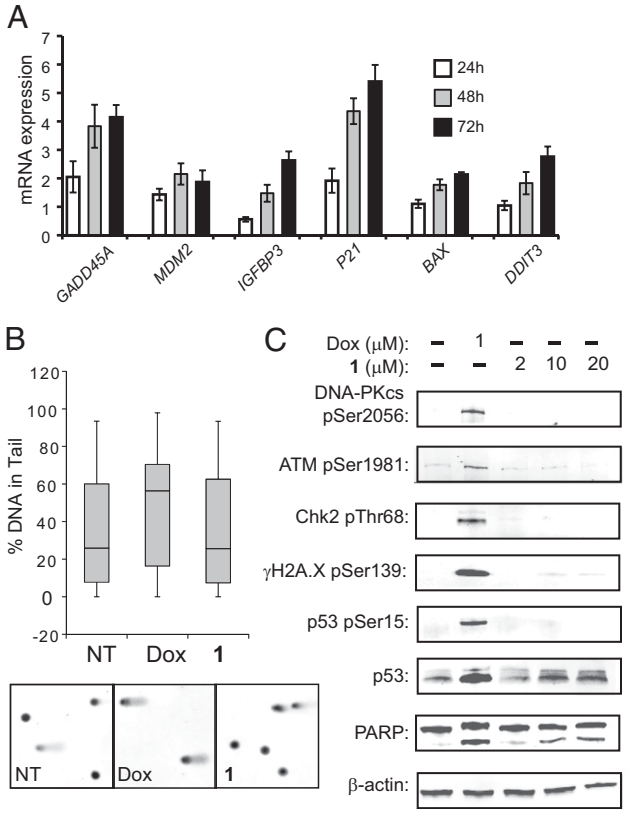

Fig. 4. Induction of p53 activity without evidence of DNA damage. (*A*) Induction of p53 target genes (*GADD45A*, *MDM2*, *IGFBP3*, *P21*, *BAX*) and DNA damage-inducible transcript 3 (DDIT3), by **1** (10 μM) at 24, 48, and 72 h. Data represent the mean of four biological replicates and error bars represent SD. (*B*) Alkaline comet assay of LNCaP cells treated with vehicle, dox (5 μM, 4 h), **1** (10 μM, 48 h). Error bars represents maximum and minimum; boxes represents the upper and lower quartiles and median. Representative comets for each treatment are shown. Effects of **1** are indistinguishable from the nontreated control, but dox treatment significantly increases comet-tail percent of DNA. $P = 0.00043$. (*C*) DNA damage markers after treatment of LNCaP cells with **1**. There is no significant phosphorylation of DNA-PKcs, ATM, Chk2, p53, or γH2A.X. Accumulation p53 and PARP cleavage are observed. Data are representative of biological triplicates except for DNA-PKcs, which was in replicate.

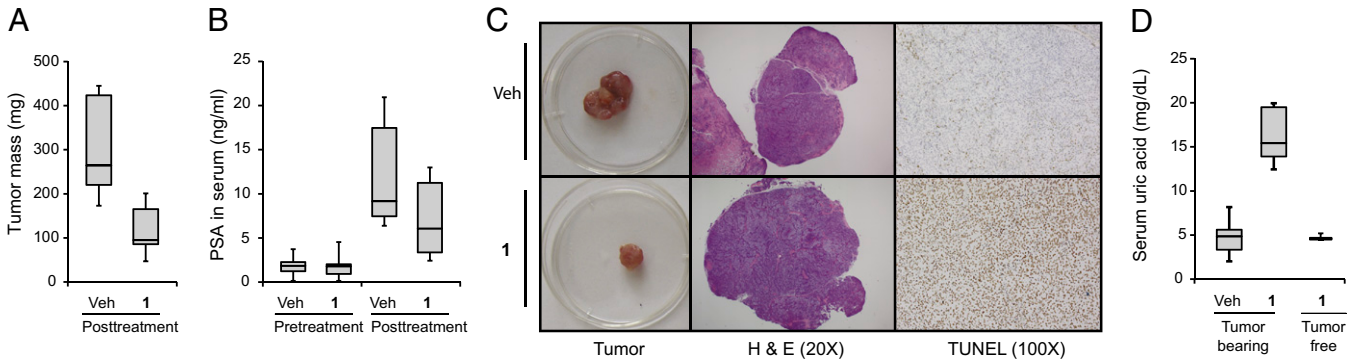

Fig. 5. Polyamide **1** demonstrates antitumor activity in prostate cancer xenografts. (*A*) Male immunocompromised mice were engrafted with LNCaP cells and observed until tumors reached ~100 mm^3. Tumor-bearing mice were then treated with 20 nmol **1** ($n = 12$) or vehicle ($n = 13$) by subcutaneous injections into the flank distal to the tumor once every 3 d for a total of three injections. Mice were killed and tumors resected and weighed 2 d after the final injection. Tumors from mice treated with **1** were smaller (mean: 112 mg; median: 94 mg; range: 47–201 mg) than those of vehicle treated mice (mean: 310 mg; median: 292 mg; range: 173–440 mg). Error bars represents maximum and minimum; boxes represents the upper and lower quartiles and median. $P = 1.6E\text{-}5$. (*B*) Serum PSA measured by ELISA pre- and posttreatment. Serum PSA is lower in the posttreatment serum of mice treated with **1** compared with vehicle. $P = 0.024$. (*C*) Selected tumors and histological stains of tumor cross-sections from mice treated with vehicle or **1**. (*D*) Treatment of LNCaP tumor bearing mice with **1** increases serum uric acid compared with vehicle controls and polyamide-treated, nontumor-bearing mice. $P = 3.2E\text{-}9$.

RPB1 in LNCaP cells was found to decrease in both a time- and concentration-dependent manner when treated with polyamide **1**. Polyamide **2**, a more cytotoxic analog of **1**, also reduced cellular RPB1 in LNCaP cells and induced cell death. Cotreatment of **2** with a proteasomal inhibitor MG132 was able to prevent the degradation of RPB1 and reduce the toxicity of **2** in cell culture. In addition, the cytotoxic effects of other RNAP2 inhibitors are reported to be attenuated by preventing S-phase entry. LNCaP cells arrested in G_0/G_1 by serum starvation also exhibited reduced sensitivity to **2** compared with cells grown in normal media. The finding that cytotoxicity is partially rescued by MG132 treatment and G_0/G_1 arrest suggests RPB1 degradation contributes to cytotoxicity; however, contributions from other DNA-dependent processes are not ruled out.

Although transcription inhibition can activate p53 signaling, both events can be caused by DNA damage. Analysis of previously published microarray data revealed the induction of several p53 target genes in LNCaP cells cotreated with DHT and **1** (12). Further validation of transcript levels of the genes in this study also showed a time-dependent increase in the expression of *GADD45A*, *MDM2*, *IGFBP3*, *P21*, *BAX*, and *DDIT3* (Fig. 4*A*). Because these genes are also markers of genotoxic stress (24) and were found to be induced in A549 cells treated with alkylating polyamide derivatives (25), we searched for signs of DNA damage to determine if it was causing transcription inhibition and p53 activation. Interestingly, both comet assay and immunblot analysis of cellular DNA damage markers showed no significant signs of DNA damage. Although faint phosphorylation of γH2A.X was visible, it is likely caused by cellular apoptosis as indicated by the concurrent PARP cleavage. These data are consistent with studies in yeast mutants that are hypersensitive to DNA damage, which showed no increased sensitivity to polyamide treatment, suggesting these reversible DNA binders do not compromise genomic integrity (30).

The activation of p53 by transcription inhibition in the absence of DNA damage has been observed for DNA-independent inhibitors of RNAP2, such as DRB, α-amanitin, and various RNAP2-targeted antibodies (5, 6, 26). Distamycin A, the natural product that provided the structural inspiration for Py-Im polyamides, inhibits the initiation of RNA synthesis in cell-free assays (27). In cell culture, distamycin also induces degradation of RPB1 and activates p53 (31, 32). However, low antitumor potency and poor stability limit its utility.

To assess the therapeutic potential of polyamide **1** as an antitumor agent, LNCaP xenografts in a murine model were treated with **1** or PBS vehicle. After three rounds of treatment, tumor growth was reduced by 64% in the treated group. Although treatment with **1** alone did not cause changes in animal body weight or obvious signs of toxicity in tumor-free animals, treatment in tumor-bearing animals resulted in weight loss after three treatments. The accompanied elevation in serum uric acid may be an indication of tumor lysis syndrome (33), which is associated with rapid tumor cell turnover upon polyamide treatment. We anticipate that Py-Im polyamides could also demonstrate efficacy in additional xenograft models.

Methods

Compounds and Reagents. Py-Im polyamides **1**, **2**, and **3** were synthesized on oxime resin, as described previously (28, 34, 35). (R)-MG132 (MG132) was from Santa Cruz Biotechnology.

Cell Viability Assays. LNCaP cells were plated in clear bottom 96-well plates at 5,000–7,500 cells per well. The cells were allowed to adhere for 24–36 h before compounds were added in fresh media. Cell viability was determined by the WST-1 assay (Roche) for **1** and **2** after 24- or 72-h incubation with cells. Cells in cytotoxicity rescue experiments were treated with **2** alone or with 3 μM MG132 for 24 h. For cell-cycle arrest experiments, LNCaP cells were seeded at 2,500–5,000 cells per well in normal media and allowed to adhere for 24–36 h. The media was replaced with normal media or media supplemented with 0.5% (vol/vol) FBS and incubated for 48 h before treatment with compound.

In Vivo Xenograft Experiments. All mice experiments were conducted under an approved protocol by the Institutional Animal Care and Use Committee of the California Institute of Technology. Male NSG mice were purchased from The Jackson Laboratory. The animals were individually caged and maintained on a standard light-dark cycle. NSG mice were engrafted with LNCaP cells (2.5 million cells) in a mixture of 1:1 media and matrigel in the left flank. Tumors were grown to ~100 mm^3 ($L \times W^2$) before beginning treatment with compound or vehicle. Py-Im polyamide **1** was administered once every 3 d at 20 nmol per animal (~1 mg/kg) in a 5% (vol/vol) DMSO:PBS vehicle solution until the experiment endpoint.

Serum Measurements. To investigate if polyamide **1** could be detected in peripheral blood after subcutaneous injections, 120 nmol of **1** [in 5% (vol/vol) DMSO/PBS] was injected into the right flank of four C57BL/6J mice. Blood was collected from anesthetized mice via retroorbital collection at 5 min, 4 h, and 12 h after injection, then processed by methods previously described and analyzed by HPLC (36). For measurement of serum PSA (KLK3) and uric acid, blood was collected from anesthetized mice via retroorbital

collection at experimental endpoint and serum was separated from blood by centrifugation. Serum PSA (KLK3) was measured by ELISA (R&D Systems) according to the manufacturer's instructions. Uric acid was measured as previously described (37).

Chromatin Immunoprecipitation. Genomic occupancy of RNAP2 was determined by ChIP with the 4H8 antibody (Abcam). LNCaP cells were plated at 35 million cells per plate in RPMI supplemented with 10% (vol/vol) CTFBS and allowed to adhere for 24–36 h. The cells were treated with compound **1** in fresh media (10% CTFBS) for 48 h. Cells treated and untreated with **1** were incubated with 1 nM DHT for 6 h. Two-step cross-linking was performed as previously described (38). After DSG removal, chromatin was immunoprecipitated by previously published methods (39). DNA was harvested by phenol chloroform extraction and purified with the QIAquick purification kit (Qiagen). Quantitative PCR was used to validate enrichment at the GAPDH transcription start site (Primers: F-GGTTTCTCTCCGCCCGTCTT, R-TGTTCGACAGTCAGCCGCAT) compared with an internal negative locus (Primers: F-TAGAAGGGGGATAGGGGAAC, R-CCAGAAAACTGGCTCCTTCTT). Each sample was immunoprecipated as five technical replicates. The three most consistent samples were combined and submitted for sequencing on an Illumina genome analyzer. Biological replicates were acquired.

Data Processing and Analysis. Sequencing reads were trimmed down to 36 bp and then mapped against the male set of human chromosomes (excluding all random chromosomes and haplotypes) using the hg19 version of the human genome as a reference. Bowtie 0.12.7 was used for aligning reads (40), with the following settings: "-v 2 -t–best–strata". Signal profiles over genomic locations were generated using custom written python scripts; the refSeq annotation was used for gene coordinates. Enhancers and promoters were defined using previously published histone marker data (41). ChIP-seq peaks were called using MACS2 with default settings (42). Enhancers were defined as $H3K4me1^+$ regions that did not intersect with $H3K4me3^+$ regions and promoters as $H3K4me3^+$ regions that did not intersect with $H3K4me1^+$ regions. Clustering was performed with Cluster 3.0 (43) and visualized with Java TreeView (44).

Comet Assay. LNCaP cells were plated at 1 million cells per 10-cm plate and allowed to adhere for 24–36 h. Cells were then incubated with either 10 μM **1** for 48 h or 5 μM doxorubicin for 4 h. DNA damage was assayed using the Trevigen CometAssay system and samples were prepared from harvested cells according to the manufacture protocol. Comets were imaged on a confocal microscope (Exciter, Zeiss) at 10× magnification. Percentage of DNA in the tail was determined using Comet Assay Lite IV (Perceptive Instruments). More than 100 comets were scored for each condition.

Immunoblot Assay. Samples for immunoblot analysis were prepared by plating LNCaP or DU145 cells at 1 million cells per 10-cm plate. Cells were allowed to adhere for 24–36 h before incubation with compound. After the appropriate incubation time, cells were washed once with ice-cold PBS and harvested in ice-cold 125 μL lysis buffer (50 mM Tris•HCl pH 7.4, 150 mM NaCl, 1 mM EDTA, 1% Triton X 100) containing protease inhibitor mixture (Roche), 1 mM PMSF (Sigma), and phosphatase inhibitors (Sigma). Samples were incubated on ice for 10 min with vortexing once every 3 min. Cellular debris was pelleted by spinning at 21,000 × *g* for 15 min to collect the supernatant. Samples were then quantified for protein content with the Bradford assay (Bio-Rad) and boiled with 4× sample buffer (Li-Cor) for 5 min. Protein electrophoresis was performed in 4–20% precast Tris•glycine SDS gels (Bio-Rad) and transferred to PVDF membranes. Membrane blocking was done with Odyssey Blocking Buffer (Li-Cor). The following antibodies used to probe changes in protein levels or phosphorylation states: RBP1 (Santa Cruz Biotechnology; N20), p53 (Santa Cruz Biotechnology; DO1), phospho-Chk2-Thr68 (Cell Signaling Technology), Phospho-p53-Ser15 (Cell Signaling Technology), phospho-H2A.X-Ser139 (Cell Signaling Technology), phosphor-ATM-Ser1981 (Abcam), phospho-DNA-PKcs-Ser2056 (Abcam), and β-actin (Abcam). Near-IR secondary antibodies (Li-Cor) were used for imaging. Experiments were performed in biological triplicate except for DNA-PKcs (replicate).

Flow Cytometry. To determine cell cycle distribution of LNCaP cells grown in normal media or under serum-starved conditions, 1 million cells were seeded to each 10-cm plate and allowed to adhere for 24–36 h. Media was then replaced with fresh normal media [10% (vol/vol) FBS] or serum-starved media [0.5% (vol/vol) FBS] and incubated for an additional 48 h. Cells were then trypsinized and prepared for analysis as previously described (45). Samples were analyzed in biological triplicate on a FACSCalibur (Becton-Dickinson) instrument. Data analysis was performed using FlowJo 7.6.5.

Quantitative RT-PCR. RNA was extracted using RNEasy columns (Qiagen) according to the manufacturer's protocols. cDNA was generated from RNA by reverse transcriptase (Transcriptor First Strand cDNA kit; Roche). Quantitative real-time RT-PCR was performed using SYBR Green PCR Master Mix (Applied Biosystems) on an ABI 7300 instrument. mRNA was measured relative to β-glucuronidase as an endogenous control. Experiments were performed in biological quadruplicates. For primer sequences see Table S1.

Confocal Microscopy. Cells were plated in 35-mm optical dishes (MatTek) and dosed with polyamide **3** at 2 μM for 24 h with or without 3μM MG132. Cells were then washed with PBS and imaged on a confocal microscope (Exciter; Zeiss) using a 63× oil immersion lens. Confocal imaging was performed following established protocols (34).

Histology and Immunohistochemistry. Tumors were resected immediately after euthanasia and fixed in neutral buffered formalin. Selected samples were embedded in paraffin, sectioned and stained with H&E. Selected sections were assessed by TUNEL, as previously described (46).

Thermal Denaturation Assays. Polyamides **1** and **2** were incubated with duplex DNA 5′-CGATGTTCAAGC-3′, which contains the predicted target site for these compounds (underlined). Melting temperature analyses were performed on a Varian Cary 100 spectrophotometer as described (47). Melting temperatures were defined as a maximum of the first derivative of absorbance at 260 nm over the range of temperatures.

Statistical Analysis. Statistical significance was calculated using the Student *t* test with two tailed variance. Results were considered significant when $P < 0.05$.

ACKNOWLEDGMENTS. We thank Rochelle Diamond of the Caltech Flow Cytometry Cell Sorting Facility for help with flow cytometry experimental setup and data acquisition; and Dr. Janet Baer, Dr. Karen L. Lencioni, and Gwen E. Williams for helpful discussions and technical assistance with animal experiments. This work was supported in part by the National Institutes of Health Grants GM27681 and HG004576, and by the Prostate Cancer Foundation. N.G.N. acknowledges the Jonsson Cancer Center Foundation at University of California at Los Angeles for continued support.

1. Derheimer FA, Chang CW, Ljungman M (2005) Transcription inhibition: A potential strategy for cancer therapeutics. *Eur J Cancer* 41(16):2569–2576.
2. Koumenis C, Giaccia A (1997) Transformed cells require continuous activity of RNA polymerase II to resist oncogene-induced apoptosis. *Mol Cell Biol* 17(12):7306–7316.
3. Jung Y, Lippard SJ (2006) RNA polymerase II blockage by cisplatin-damaged DNA. Stability and polyubiquitylation of stalled polymerase. *J Biol Chem* 281(3):1361–1370.
4. Ljungman M, Zhang FF (1996) Blockage of RNA polymerase as a possible trigger for u.v. light-induced apoptosis. *Oncogene* 13(4):823–831.
5. Ljungman M, Zhang FF, Chen F, Rainbow AJ, McKay BC (1999) Inhibition of RNA polymerase II as a trigger for the p53 response. *Oncogene* 18(3):583–592.
6. Arima Y, et al. (2005) Transcriptional blockade induces p53-dependent apoptosis associated with translocation of p53 to mitochondria. *J Biol Chem* 280(19):19166–19176.
7. Nguyen VT, et al. (1996) In vivo degradation of RNA polymerase II largest subunit triggered by alpha-amanitin. *Nucleic Acids Res* 24(15):2924–2929.
8. Arseneau JC, et al. (1972) Nonlymphomatous malignant tumors complicating Hodgkin's disease. Possible association with intensive therapy. *N Engl J Med* 287(22):1119–1122.
9. Dervan PB, Edelson BS (2003) Recognition of the DNA minor groove by pyrrole-imidazole polyamides. *Curr Opin Struct Biol* 13(3):284–299.
10. Chenoweth DM, Dervan PB (2009) Allosteric modulation of DNA by small molecules. *Proc Natl Acad Sci USA* 106(32):13175–13179.
11. Chenoweth DM, Dervan PB (2010) Structural basis for cyclic Py-Im polyamide allosteric inhibition of nuclear receptor binding. *J Am Chem Soc* 132(41):14521–14529.
12. Nickols NG, Dervan PB (2007) Suppression of androgen receptor-mediated gene expression by a sequence-specific DNA-binding polyamide. *Proc Natl Acad Sci USA* 104 (25):10418–10423.
13. Nickols NG, Jacobs CS, Farkas ME, Dervan PB (2007) Modulating hypoxia-inducible transcription by disrupting the HIF-1-DNA interface. *ACS Chem Biol* 2(8):561–571.
14. Muzikar KA, Nickols NG, Dervan PB (2009) Repression of DNA-binding dependent glucocorticoid receptor-mediated gene expression. *Proc Natl Acad Sci USA* 106(39): 16598–16603.
15. Raskatov JA, et al. (2012) Modulation of NF-κB-dependent gene transcription using programmable DNA minor groove binders. *Proc Natl Acad Sci USA* 109(4):1023–1028.

16. Matsuda H, et al. (2011) Transcriptional inhibition of progressive renal disease by gene silencing pyrrole-imidazole polyamide targeting of the transforming growth factor-β1 promoter. *Kidney Int* 79(1):46–56.
17. Synold TW, et al. (2012) Single-dose pharmacokinetic and toxicity analysis of pyrrole-imidazole polyamides in mice. *Cancer Chemother Pharmacol* 70(4):617–625.
18. Raskatov JA, et al. (2012) Gene expression changes in a tumor xenograft by a pyrrole-imidazole polyamide. *Proc Natl Acad Sci USA* 109(40):16041–16045.
19. Palstra RJ, et al. (2008) Maintenance of long-range DNA interactions after inhibition of ongoing RNA polymerase II transcription. *PLoS ONE* 3(2):e1661.
20. Bregman DB, et al. (1996) UV-induced ubiquitination of RNA polymerase II: A novel modification deficient in Cockayne syndrome cells. *Proc Natl Acad Sci USA* 93(21): 11586–11590.
21. Ratner JN, Balasubramanian B, Corden J, Warren SL, Bregman DB (1998) Ultraviolet radiation-induced ubiquitination and proteasomal degradation of the large subunit of RNA polymerase II. Implications for transcription-coupled DNA repair. *J Biol Chem* 273(9):5184–5189.
22. Aune GJ, et al. (2008) Von Hippel-Lindau-coupled and transcription-coupled nucleotide excision repair-dependent degradation of RNA polymerase II in response to trabectedin. *Clin Cancer Res* 14(20):6449–6455.
23. McKay BC, Becerril C, Spronck JC, Ljungman M (2002) Ultraviolet light-induced apoptosis is associated with S-phase in primary human fibroblasts. *DNA Repair (Amst)* 1(10):811–820.
24. el-Deiry WS (1998) Regulation of p53 downstream genes. *Semin Cancer Biol* 8(5): 345–357.
25. Kashiwazaki G, et al. (2012) Synthesis and biological properties of highly sequence-specific-alkylating N-methylpyrrole-N-methylimidazole polyamide conjugates. *J Med Chem* 55(5):2057–2066.
26. Derheimer FA, et al. (2007) RPA and ATR link transcriptional stress to p53. *Proc Natl Acad Sci USA* 104(31):12778–12783.
27. Puschendorf B, Petersen E, Wolf H, Werchau H, Grunicke H (1971) Studies on the effect of distamycin A on the DNA dependent RNA polymerase system. *Biochem Biophys Res Commun* 43(3):617–624.
28. Meier JL, Montgomery DC, Dervan PB (2012) Enhancing the cellular uptake of Py-Im polyamides through next-generation aryl turns. *Nucleic Acids Res* 40(5):2345–2356.
29. Carlson CD, et al. (2010) Specificity landscapes of DNA binding molecules elucidate biological function. *Proc Natl Acad Sci USA* 107(10):4544–4549.
30. Marini NJ, et al. (2003) DNA binding hairpin polyamides with antifungal activity. *Chem Biol* 10(7):635–644.
31. Zhang Z, et al. (2009) Tanshinone IIA triggers p53 responses and apoptosis by RNA polymerase II upon DNA minor groove binding. *Biochem Pharmacol* 78(10): 1316–1322.
32. Hirota M, Fujiwara T, Mineshita S, Sugiyama H, Teraoka H (2007) Distamycin A enhances the cytotoxicity of duocarmycin A and suppresses duocarmycin A-induced apoptosis in human lung carcinoma cells. *Int J Biochem Cell Biol* 39(5):988–996.
33. Coiffier B, Altman A, Pui CH, Younes A, Cairo MS (2008) Guidelines for the management of pediatric and adult tumor lysis syndrome: An evidence-based review. *J Clin Oncol* 26(16):2767–2778.
34. Best TP, Edelson BS, Nickols NG, Dervan PB (2003) Nuclear localization of pyrrole-imidazole polyamide-fluorescein conjugates in cell culture. *Proc Natl Acad Sci USA* 100(21):12063–12068.
35. Puckett JW, Green JT, Dervan PB (2012) Microwave assisted synthesis of Py-Im polyamides. *Org Lett* 14(11):2774–2777.
36. Raskatov JA, Hargrove AE, So AY, Dervan PB (2012) Pharmacokinetics of Py-Im polyamides depend on architecture: Cyclic versus linear. *J Am Chem Soc* 134(18): 7995–7999.
37. Dai KS, et al. (2005) An evaluation of clinical accuracy of the EasyTouch blood uric acid self-monitoring system. *Clin Biochem* 38(3):278–281.
38. Nowak DE, Tian B, Brasier AR (2005) Two-step cross-linking method for identification of NF-kappaB gene network by chromatin immunoprecipitation. *Biotechniques* 39(5): 715–725.
39. Reddy TE, et al. (2009) Genomic determination of the glucocorticoid response reveals unexpected mechanisms of gene regulation. *Genome Res* 19(12):2163–2171.
40. Langmead B, Trapnell C, Pop M, Salzberg SL (2009) Ultrafast and memory-efficient alignment of short DNA sequences to the human genome. *Genome Biol* 10(3):R25.
41. Yu JD, et al. (2010) An integrated network of androgen receptor, polycomb, and TMPRSS2-ERG gene fusions in prostate cancer progression. *Cancer Cell* 17(5):443–454.
42. Zhang Y, et al. (2008) Model-based Analysis of ChIP-Seq (MACS). *Genome Biol* 9(9): R137.
43. de Hoon MJ, Imoto S, Nolan J, Miyano S (2004) Open source clustering software. *Bioinformatics* 20(9):1453–1454.
44. Saldanha AJ (2004) Java Treeview—Extensible visualization of microarray data. *Bioinformatics* 20(17):3246–3248.
45. Diamond RA, DeMaggio S (2000) *In Living Color: Protocols in Flow Cytometry and Cell Sorting* (Springer, Berlin, New York), pp xxv, 800 pp.
46. Zisman A, et al. (2003) LABAZ1: A metastatic tumor model for renal cell carcinoma expressing the carbonic anhydrase type 9 tumor antigen. *Cancer Res* 63(16): 4952–4959.
47. Dose C, Farkas ME, Chenoweth DM, Dervan PB (2008) Next generation hairpin polyamides with (R)-3,4-diaminobutyric acid turn unit. *J Am Chem Soc* 130(21): 6859–6866.